frontiers | Frontiers in Nanotechnology

TYPE Original Research
PUBLISHED 05 February 2024
DOI 10.3389/fnano.2023.1333127

OPEN ACCESS

EDITED BY
Estela Blaisten-Barojas,
George Mason University, United States

REVIEWED BY
Erick Ulin-Avila,
Center for Engineering and Development CIDESI, Mexico
Filippo Fabbri,
National Research Council (CNR), Italy

*CORRESPONDENCE
Antonija Grubišić-Čabo,
a.grubisic-cabo@rug.nl
Michael S. Fuhrer,
michael.fuhrer@monash.edu

RECEIVED 04 November 2023
ACCEPTED 21 December 2023
PUBLISHED 05 February 2024

CITATION
Grubišić-Čabo A, Kotsakidis JC, Yin Y, Tadich A, Haldon M, Solari S, Riley J, Huwald E, Daniels KM, Myers-Ward RL, Edmonds MT, Medhekar NV, Gaskill DK and Fuhrer MS (2024), Quasi-freestanding AA-stacked bilayer graphene induced by calcium intercalation of the graphene-silicon carbide interface. *Front. Nanotechnol.* 5:1333127. doi: 10.3389/fnano.2023.1333127

Quasi-freestanding AA-stacked bilayer graphene induced by calcium intercalation of the graphene-silicon carbide interface

Antonija Grubišić-Čabo[1,2]*, Jimmy C. Kotsakidis[1,3], Yuefeng Yin[4,5], Anton Tadich[5,6,7], Matthew Haldon[1], Sean Solari[1], John Riley[7], Eric Huwald[7], Kevin M. Daniels[8,9,10], Rachael L. Myers-Ward[11], Mark T. Edmonds[1,5], Nikhil V. Medhekar[4,5], D. Kurt Gaskill[9] and Michael S. Fuhrer[1,5]*

[1]School of Physics and Astronomy, Monash University, Clayton, VIC, Australia, [2]Zernike Institute for Advanced Materials, University of Groningen, Groningen, Netherlands, [3]Laboratory for Physical Sciences, College Park, MD, United States, [4]Department of Materials Science and Engineering, Monash University, Clayton, VIC, Australia, [5]ARC Centre of Excellence in Future Low Energy Electronics Technologies (FLEET), Monash University, Clayton, VIC, Australia, [6]Australian Synchrotron, Melbourne, VIC, Australia, [7]Department of Physics, La Trobe University, Melbourne, VIC, Australia, [8]Department of Electrical and Computer Engineering, University of Maryland, College Park, MD, United States, [9]Institute for Research in Electronics and Applied Physics, University of Maryland, College Park, MD, United States, [10]Fischell Institute for Biomedical Devices, University of Maryland, College Park, MD, United States, [11]US Naval Research Laboratory, Washington, DC, United States

We study quasi-freestanding bilayer graphene on silicon carbide intercalated by calcium. The intercalation, and subsequent changes to the system, were investigated by low-energy electron diffraction, angle-resolved photoemission spectroscopy (ARPES) and density-functional theory (DFT). Calcium is found to intercalate only at the graphene-SiC interface, completely displacing the hydrogen terminating SiC. As a consequence, the system becomes highly n-doped. Comparison to DFT calculations shows that the band dispersion, as determined by ARPES, deviates from the band structure expected for Bernal-stacked bilayer graphene. Instead, the electronic structure closely matches AA-stacked bilayer graphene on calcium-terminated SiC, indicating a spontaneous transition from AB- to AA-stacked bilayer graphene following calcium intercalation of the underlying graphene-SiC interface.

KEYWORDS

graphene, calcium, intercalation, electronic structure, ARPES, DFT

1 Introduction

Graphene, a single layer of graphite Novoselov et al. (2004) is notable for its unique bandstructure with massless Dirac Fermions Novoselov et al. (2005), which give rise to a plethora of exotic physical phenomena, such as a π-Berry phase Zhang et al. (2005); Liu et al. (2011); Hwang et al. (2011), Katsnelson et al. (2006) and an unusual quantum Hall effect Zhang et al. (2005).

In contrast, the most typical form of bilayer graphene, so called AB- or Bernal stacked bilayer graphene (Supplementary Figures S3A, B), has a completely different electronic structure with massive, yet gapless, Dirac fermions, and a Berry phase of 2π Ohta et al. (2006); Partoens and Peeters (2006); McCann and Koshino (2013); Novoselov et al. (2006). In principle, other types of stacking, such as AA-stacking (Supplementary Figures S3C, D), exist. AA-stacking is a metastable stacking, where graphene layers lie directly above one another. Consequently, AA-stacked graphene has an electronic structure which can be considered as a superposition of two single-layer spectra, preserving massless Dirac fermions and a π-Berry phase Liu et al. (2009); Rozhkov et al. (2016). Despite many interesting properties predicted for AA-stacked bilayer graphene, including a recent prediction that it might host a fractional metal state Sboychakov et al. (2021), there are very few experimental realisations Kim et al. (2013); Liu et al. (2009); Caffrey et al. (2016); Endo et al. (2018); de Jong et al. (2018), de Jong et al. (2023). Out of the few reported cases, the majority have been found in lithium intercalated systems Caffrey et al. (2016); Endo et al. (2018), or contained within very small regions otherwise surrounded by AB-stacked graphene de Jong et al. (2018), de Jong et al. (2023).

One of the most promising methods for graphene production in terms of scalability is the growth of graphene on silicon carbide (SiC) which allows formation of large-scale graphene with high carrier mobility Starke and Riedl (2009); Nyakiti et al. (2012); Kruskopf et al. (2016); Emtsev et al. (2009). Graphene on SiC can either be epitaxial, i.e., directly grown on the SiC, with a buffer layer in between the graphene and the SiC interface, or quasi-freestanding graphene–most commonly created via hydrogen intercalation of epitaxial graphene Daniels et al. (2017); Riedl et al. (2009), in which graphene retains the properties expected for the isolated layer Sforzini et al. (2015). Hydrogen is not the only element that can be used to create quasi-freestanding graphene on SiC by means of intercalation Briggs et al. (2019); various other elements can be used, such as gold Sohn et al. (2021); Marchenko et al. (2016), iron Sung et al. (2014); Shen et al. (2018), oxygen Oliveira et al. (2013), lithium Bao et al. (2014); Caffrey et al. (2016); Endo et al. (2018); Virojanadara et al. (2010), magnesium Kotsakidis et al. (2020); Grubišić-Čabo et al. (2021); Kotsakidis et al. (2021), calcium Kotsakidis et al. (2020); Valla et al. (2009); Yang et al. (2014); Endo et al. (2020); Toyama et al. (2022); Ichinokura et al. (2016), antimony Wolff et al. (2019) and ytterbium Watcharinyanon et al. (2013). The majority of the intercalation studies have been done on epitaxial monolayer and bilayer graphene on SiC, with very few intercalation studies on already quasi-freestanding, hydrogen intercalated, graphene Watcharinyanon et al. (2012); Kim et al. (2019); Kotsakidis et al. (2020). Of particular interest to us is calcium intercalated graphene, whose study was inspired by the bulk superconducting graphite intercalation compound CaC_6 Sugawara et al. (2009); Yang et al. (2014); Weller et al. (2005); Emery et al. (2005). The majority of calcium intercalation experiments have been performed on graphene grown on SiC, as this allows for growth of large-area graphene that can be characterised with various surface characterisation techniques, such as X-ray photoelectron spectroscopy (XPS), angle-resolved photoemission spectroscopy (ARPES), low-energy electron diffraction (LEED) and scanning tunnelling microscopy Kotsakidis et al. (2020); Ohta et al. (2006); Kanetani et al. (2012); McChesney et al. (2010). Calcium intercalation is known to strongly n-type dope graphene, an effect which has been extensively studied Ohta et al. (2006); McChesney et al. (2010), however, the impact of calcium intercalation on the structural aspects of graphene and the precise positioning of calcium atoms remained somewhat ambiguous Kotsakidis et al. (2020); Ichinokura et al. (2016); Kanetani et al. (2012). Recent research using XPS by Kotsakidis et al. (2020) has shed light on this, revealing that calcium is situated at the interface between the SiC substrate and graphene buffer layer, with work by Toyama et al. (2022) further confirming that calcium prefers to go to the SiC interface.

In this paper, we report calcium intercalation of quasi-freestanding bilayer graphene (QFSBLG) on SiC. Using a combination of LEED, ARPES and density-functional theory (DFT), calcium is found to intercalate only at the interface between graphene and SiC, fully replacing hydrogen in the structure, and not between the graphene layers. This results in highly n-doped, quasi-freestanding bilayer graphene (Ca-QFSBLG) with a drastically altered electronic structure, as seen by ARPES. Comparison with DFT shows the structure to be in close agreement with AA-stacked bilayer graphene, indicating a spontaneous transition from AB- to AA-stacking, which has not been previously observed for calcium intercalated graphene.

2 Materials and methods

2.1 Sample preparation

QFSBLG samples on SiC were grown on semi-insulating 6H-SiC(0001) substrate as described in Ref. Daniels et al. (2017). Sample preparation, ARPES and LEED measurements were carried out at the Toroidal Analyzer endstation at the Soft X-ray Beamline of the Australian Synchrotron. Samples were introduced to ultra-high vacuum (UHV, base pressure of 1×10^{-10} mbar), and annealed over night at 773–823 K. Sample cleanliness was confirmed by LEED and ARPES. A calcium effusion cell was baked at 423 K overnight and outgassed at 588 K. Once the pressure reached 1×10^{-8} mbar, the effusion cell was inserted into the UHV preparation chamber. Calcium (dendritic pieces, 99.99%, Sigma-Aldrich) was intercalated under graphene following modified recipe from Ref. Kotsakidis et al. (2020): Calcium was evaporated for 15 min, with the calcium cell held at 688 K, and deposited on the graphene/SiC substrate held at room temperature. The thickness of deposited calcium layer was 22 Å, as determined by a quartz crystal microbalance. Following the deposition, the graphene/SiC substrate was annealed at 773 K for 15 min, in order to facilitate calcium intercalation.

2.2 Angle-resolved photoemission spectroscopy and low-energy electron diffraction

Structural characterisation of samples was undertaken using a LEED (OCIVM 3 grid reverse view optics, 200 μm spot size) at room temperature, in the endstation used for ARPES. ARPES measurements used a toroidal-type angle-resolving endstation Broekman et al. (2005) at the Soft X-Ray Beamline of the

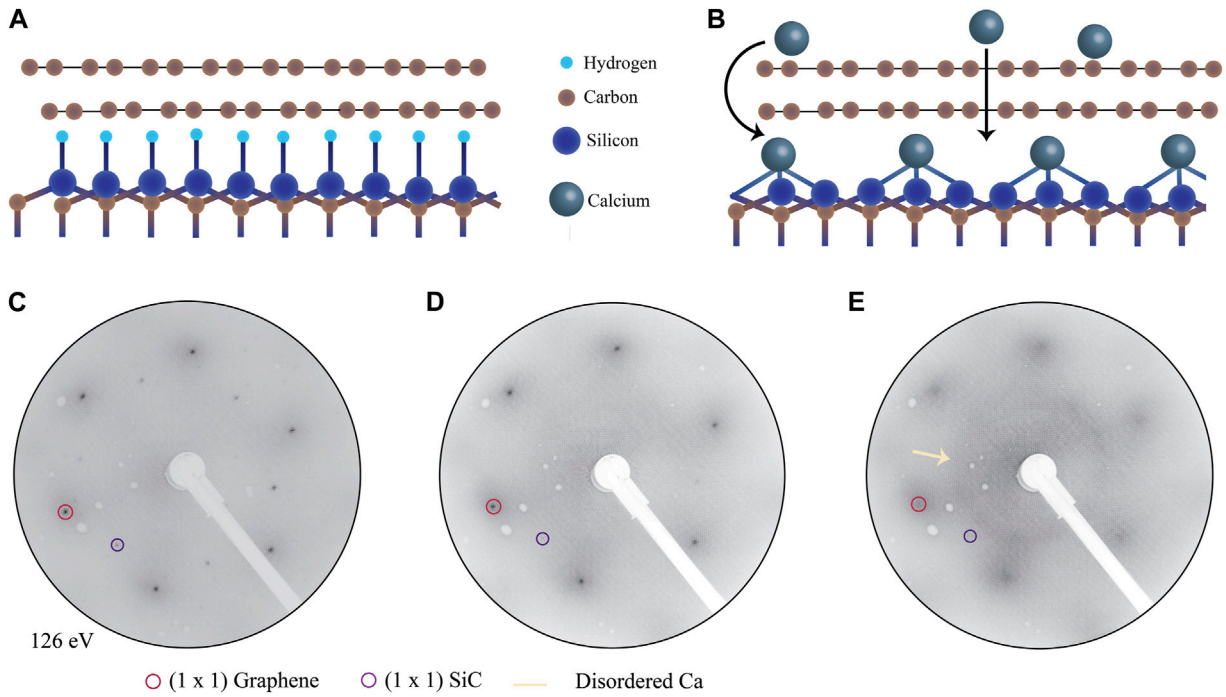

FIGURE 1
Quasi freestanding bilayer graphene (QFSBLG) before and after calcium intercalation. A sketch of QFSBLG before and after intercalation, where hydrogen is replaced by calcium at the SiC interface is shown in **(A,B)**, respectively. **(C)** LEED image of QFSBLG prior calcium intercalation, **(D)** following first, and **(E)** following second calcium intercalation. Red circles indicate the (1 × 1) graphene spots, purple circles indicate the (1 × 1) SiC spots. Yellow arrow points to the ring arising from disordered Ca. All data taken at an incident beam energy of 126 eV and room temperature.

Australian Synchrotron. All ARPES data was taken at room temperature with photon energy ($h\nu$) of 100 eV using linearly polarised light at normal incidence to the sample. The beam spot size was 100 μm × 60 μm. The binding energy (E_{Bin}) scale for all spectra is referenced to the Fermi energy (E_F), determined using the Fermi edge of a gold foil reference sample in electrical contact with the sample. The toroidal analyser permits all polar (Θ) emission angles (−90° to +90°) to be measured along a high-symmetry azimuth (ϕ) of the surface containing the $\bar{\Gamma}$ point. This unique geometry allows for measurement of the Dirac cone along the $\bar{K}$ – $\bar{\Gamma}$ – $\bar{K}$ high-symmetry direction without the need for complex alignment of the spectrometer. Under this geometry, the polarisation vector of the X-rays is entirely contained in the detection plane. The estimated momentum and energy resolution are ≈ 0.02 Å^{-1} and ≈ 150 meV.

2.3 Density-functional theory and tight-binding

First principles density-functional theory calculations were implemented using the Vienna *ab initio* Simulation Package (VASP) to calculate the electronic structure of Ca-QFSBLG Kresse and Furthmüller (1996). The Perdew-Burke-Ernzehof (PBE) form of the generalized gradient approximation (GGA) was used to describe electron exchange and correlation Perdew et al. (1996). A semi-empirical functional (DFT-D2) was employed to describe van der Waals interactions in the system Grimme et al. (2011). The kinetic energy cut-off for the plane-wave basis set was set to 500 eV. We used a 9 × 9 × 1 Γ-centred k-point mesh for sampling the Brillouin zone. The unfolded band structure and Fermi surface were obtained using the KPROJ program based on the k-projection method Chen and Weinert (2018); Chen et al. (2017). Tight-binding calculations were performed in Igor Pro Wavemetrics software based on Ref. Rozhkov et al. (2016) for AA-stacked bilayer graphene, and Refs. Partoens and Peeters (2006); McCann and Koshino (2013) for AB-stacked bilayer graphene. Tight-binding calculations are presented along the $\bar{K}$ – $\bar{\Gamma}$ – $\bar{K}$ high-symmetry direction. Parameters used for tight binding calculations were t = 3.05 (±0.05) and γ_1 = 0.4 for AB-stacked QFSBLG, and t = 2.9 (±0.05) and γ_1 = 0.4 for AA-stacked Ca-QFSBLG.

3 Results and discussion

3.1 Experimental results

QFSBLG samples, Figure 1A, prepared as described in Ref. Daniels et al. (2017) were loaded into the UHV chamber and annealed to remove surface adsorbates, as described in Methods. Following the annealing procedure, LEED data was taken on the clean sample, as shown in Figure 1C. LEED data shows typical diffraction pattern of quasi-freestanding graphene, with only (1 × 1) graphene spots (red circles) and (1 × 1) SiC spots rotated 30° with respect to graphene (purple circles) visible. Following calcium intercalation (Figure 1B), the SiC (1 × 1) spots are less intense compared to the clean QFSBLG, but no other significant changes can

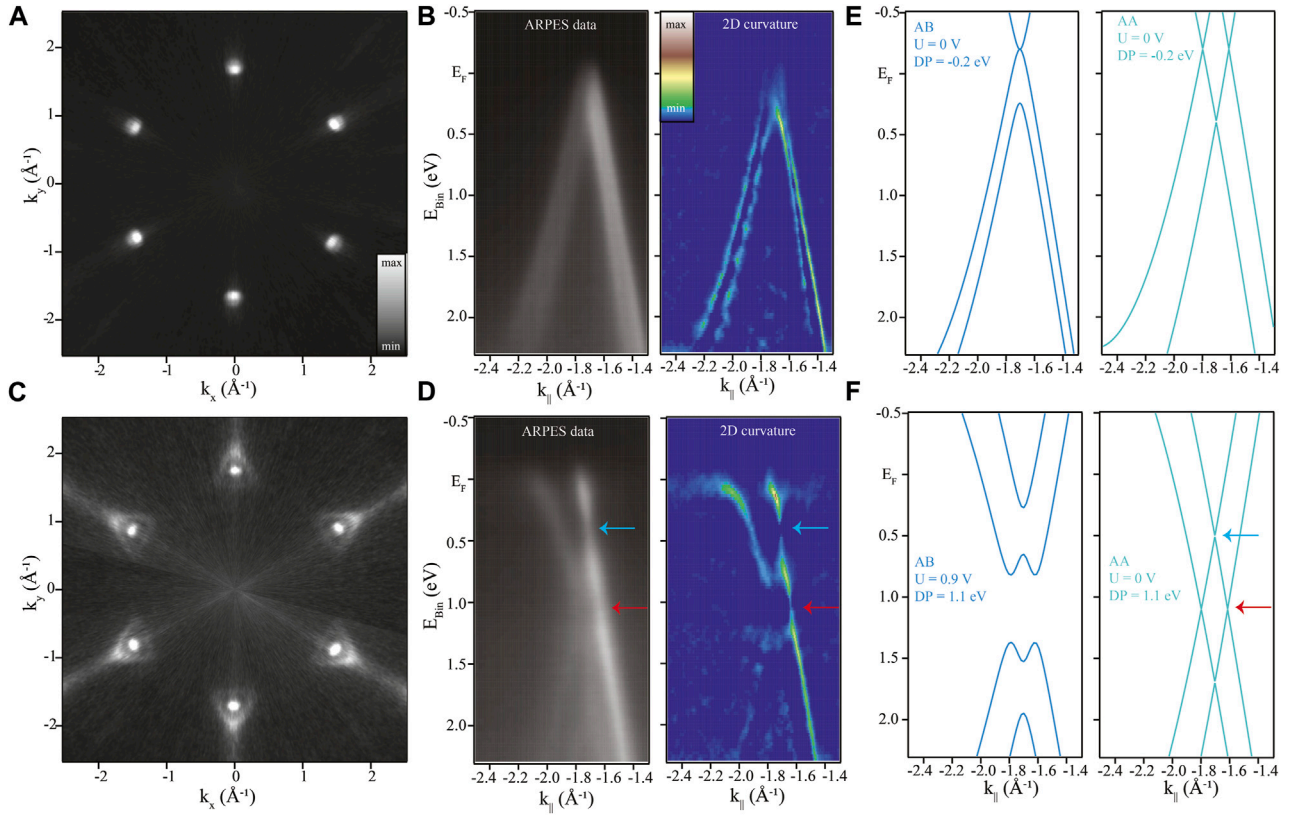

FIGURE 2
ARPES measurements of clean and calcium intercalated quasi-freestanding bilayer graphene (Ca-QFSBLG) after the first intercalation step. **(A)** Fermi surface and **(B)** band structure around the $\bar{K}$ point of QFSBLG, and **(C)** Fermi surface and **(D)** band structure around the $\bar{K}$ point of Ca-QFSBLG. In **(B,D)** both raw ARPES spectra (left) and a 2D curvature of ARPES spectra (right) are shown. Following calcium intercalation, a significant change in the electronic structure and doping level can be seen. **(E)** and **(F)** show tight-binding calculations for AB- (left) and AA-stacked (right) bilayer graphene before and after calcium intercalation, respectively. Red arrows in **(D,F)** indicate location of band crossing between the top and bottom layer band, and a lack of the band gap for AA-stacked bilayer graphene. Blue arrows in **(D,F)** show the Dirac point in the top graphene layer which appears ungapped.

be seen in LEED, as shown in Figure 1D. After the second intercalation step (Figure 1E) drastic changes can be observed in the LEED pattern: (1 × 1) SiC spots are almost completely gone, while (1 × 1) graphene spots are much weaker and broader. Blurring of the graphene (1 × 1) spots suggests additional scattering, likely from calcium atoms accumulating on the surface of the sample in a disordered manner. A new feature can also be observed in the diffraction pattern in Figure 1E, a diffuse ring, marked by a yellow arrow, with a radius corresponding to that of a $(\sqrt{3} \times \sqrt{3})R30^{\circ}$ calcium structure. Ring like features observed in LEED usually point towards rotationally disordered system Emtsev et al. (2008), suggesting calcium is not ordered either under graphene or on its surface. This is in contrast to previous LEED data on calcium intercalated graphene on SiC, where a sharp single domain $(\sqrt{3} \times \sqrt{3})R30^{\circ}$ LEED pattern coming from calcium intercalation is observed Kanetani et al. (2012); Kotsakidis et al. (2020); Toyama et al. (2022). One possible explanation for this discrepancy is that in our system, disorder comes from calcium that did not intercalate, but is instead deposited on the surface of the sample where it does not order. Another possibility is that while calcium is replacing hydrogen at the SiC interface, it does so without rotational order, though the reason for this difference in structure is not clear.

Following structural characterization by LEED, we proceed with the electronic structure investigation using ARPES Damascelli (2004) which allows direct imaging of the electronic bands. Due to an increase in observed disorder for the second intercalation step in LEED (Figure 1E) we will only focus on the first intercalation step for the ARPES investigation. Figure 2 shows intercalation induced changes in the electronic structure of graphene, as observed by ARPES. Changes are tracked in the energy–momentum cuts taken at the Fermi surface (Figures 2A, C) and along the $\bar{K} - \bar{\Gamma} - \bar{K}$ high-symmetry direction (Figures 2B, D). In order to enhance the dispersive features of graphene around the $\bar{K}$ point, we use a two-dimensional (2D) curvature analysis technique Zhang et al. (2011), shown in Figures 2B, D, on the right. The Fermi surface map, Figure 2A, shows the first Brillouin zone of pristine QFSBLG prior calcium intercalation, with six hole pockets visible at the Brillouin zone boundary. As expected for the case of bilayer graphene Ohta et al. (2006), two sets of bands are visible in the energy dispersion data, Figure 2B. Since the samples are p-doped, the Dirac point is located above the Fermi level (0.20 eV, Supplementary Material), which can be clearly seen in the energy dispersion and the 2D curvature data (Figure 2B).

Upon calcium intercalation, profound changes can be observed in the electronic structure: two sets of electron pockets can be seen at the Fermi surface (Figure 2C), and system exhibits high levels of

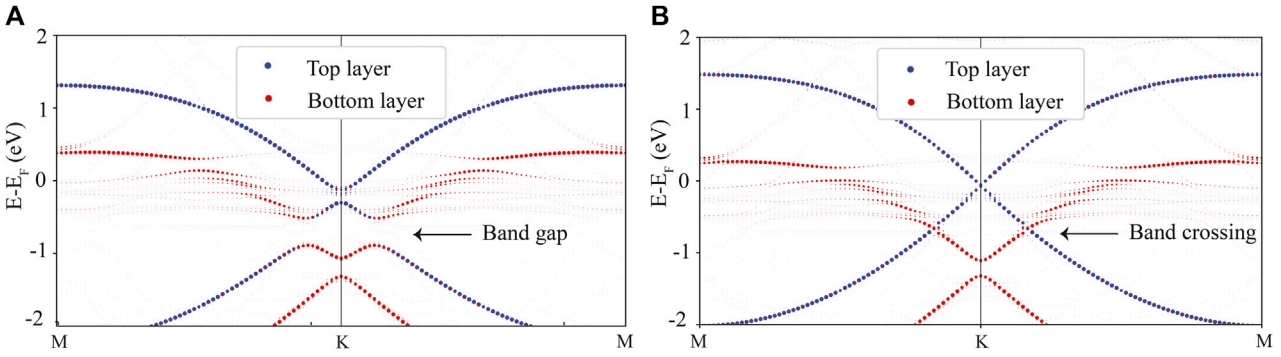

FIGURE 3
DFT calculations for calcium intercalated QFSBLG. The unfolded band structure of calcium intercalated bilayer graphene for the case of AB- and AA-stacking is shown in **(A)** and **(B)**, respectively. The contribution from the top graphene layer is shown in blue, and from the bottom layer in red. Arrows indicate a band gap for the case of AB-stacking, **(A)**, and a band crossing for the case of AA-stacking in Ca-QFSBLG, **(B)**.

n-doping (Figure 2D). In order to better understand the dispersions and changes arising from calcium intercalation, we compare our experimental data to simple tight-binding models for AA- and AB-stacked graphene (Figures 2E, F) Rozhkov et al. (2016); Partoens and Peeters (2006). The same model was used to estimate Dirac point position, doping, Fermi wavevector and Fermi velocity. We used the band position data obtained from momentum dispersion curves, to refine the tight-binding model, and select the appropriate graphene stacking. More information about this can be found in the Supplementary Material. Prior to calcium intercalation, the system is found to be p-doped, with the Dirac point located at DP = (0.20 ± 0.02) eV above the Fermi level, and a Fermi wavevector (k_F) value of k_F = (0.057 ± 0.007) Å^{-1}, corresponding to a hole carrier density of n_h^{total} = (5.17 ± 0.08) × 10^{12} cm^{-2}, in agreement with literature values for hydrogen intercalated graphene on SiC Riedl et al. (2009); Sforzini et al. (2015). Following calcium intercalation (Figures 2C, D) the sample is transformed into highly n-doped system in which no clear band gap can be seen. This structure is in stark contrast to the C_6CaC_6 electronic structure, where the ordered calcium phase gives rise to a folding of the π bands of graphene, resulting in the folded bands appearing close to the $\bar{\Gamma}$ point Kanetani et al. (2012); Toyama et al. (2022); Mazin and Balatsky (2010). In the case of Ca-QFSBLG, no states are observed at the $\bar{\Gamma}$ point, supporting the interpretation that in our case calcium is not ordered in C_6CaC_6 structure, in agreement with the LEED data (Figures 1D, E). Absence of the signatures of C_6CaC_6 structure implies that calcium is not intercalated between the layers, in agreement with recent work by Kotsakidis et al. (2020). Rather, we instead observe a quasi-freestanding bilayer graphene that is n-doped. Nevertheless, there are several discrepancies between our results (Figure 2D) and what is expected from simply n-doped (quasi-freestanding) bilayer graphene Ohta et al. (2006). The most obvious discrepancy is a lack of band gap in the system (see red and blue arrows in Figure 2D), which is expected for the simple case of AB-stacked bilayer graphene Ohta et al. (2006); Grubišić-Čabo et al. (2021). This is reminiscent of the structure expected for AA-stacked bilayer graphene where a band gap is not expected, and the electronic bands still have massless character as for the case of monolayer graphene Rozhkov et al. (2016). Taking this into the account, we modelled both AA- and AB-stacked bilayer graphene with tight-binding (Figures 2E, F) and DFT (Figure 3). From the tight-binding model, the best agreement was obtained for AA-stacked bilayer graphene, where the inner band Fermi wavevector was k_F^{inner} = (0.086 ± 0.007) Å^{-1}, and the outer band was k_F^{outer} = (0.280 ± 0.007) Å^{-1}. These values correspond to a total electron density of n_e^{total} = n_e^{inner}+n_e^{outer} = (1.37 ± 0.06) × 10^{14} cm^{-2}, a two orders of magnitude increase in carrier concentration with respect to the pristine QFSBLG. The aforementioned dramatic increase in the carrier concentration is accompanied with small reduction in Fermi velocity of graphene–Ca-QFSBLG has Fermi velocity v_F = (0.93 ± 0.02) × 10^6 ms^{-1}, while QFSBLG has Fermi velocity v_F = (0.99 ± 0.02) × 10^6 ms^{-1}, suggesting that no significant renormalisaiton of Fermi velocity due to transformation of stacking Li et al. (2010), change of the dielectric constant of the graphene's surroundings Hwang et al. (2012), or many-body interactions Elias et al. (2011) takes place. Lastly, while the observed increase in the carrier density is significant, it is lower than values observed for the case when calcium goes both to the SiC interface and in between the sheets of bilayer graphene Toyama et al. (2022), thus underpinning the notion of intercalation occurring solely at the interface of our system.

3.2 Theoretical results

We further examine the nature of stacking in Ca-QFSBLG by performing DFT calculations of the electronic structure of AB- and AA-stacked Ca-QFSBLG. We first calculate the calcium intercalation energy based on Eq. 1 as follows:

$$E_I = E(SiC/graphene) + E(Ca) - E(SiC/graphene + Ca), \quad (1)$$

where E_I is the intercalation energy, E (*SiC/graphene*), E (*Ca*) and E (*SiC/graphene* + *Ca*) are the energy of SiC/graphene heterostructure (SiC covalently bonded with graphene plus a monolayer graphene), atomic energy of calcium in its bulk state, and the energy of SiC/graphene system upon calcium intercalation, respectively. Once calcium is placed below bilayer graphene, a small difference is found in the formation energy between the AA- and AB-stacked bilayer graphene, as shown in Table 1, with AB-stacking being slightly favourable. This small difference in formation energy suggests it is plausible that AA-stacking could

TABLE 1 Calculation for intercalation energy, AA- vs. AB-stacking, using different van der Waals corrections.

Stacking type	DFT-D2 energy (eV/Ca atom)	DFT-D3 energy (eV/Ca atom)
AA	0.94	1.08
AB	0.98	1.09

indeed be a stable phase in Ca-QFSBLG, similar to what has been observed for the case of lithium intercalation Watcharinyanon et al. (2012); Caffrey et al. (2016). As both structures appear energetically stable, and are close in the formation energy, DFT band structure calculations were performed for AA- and AB-stacking in order to determine which structure fits experimental ARPES data better.

The unfolded band structure of AA- and AB-stacked Ca-QFSBLG is shown in Figure 3. For the case of AB-stacked Ca-QFSBLG (Figure 3A), a large band gap, approximately 0.38 eV in size, is found between the top of the valence band and bottom of a conduction band, situated 0.51 eV below the Fermi level. This structure is similar to the one observed for magnesium intercalated graphene on SiC Grubišić-Čabo et al. (2021), where a band gap of 0.36 eV was observed. In the case of AA-stacked bilayer graphene (Figure 3B), the structure is markedly different, and no band gap is found between the top of the valence band and bottom of a conduction band. Instead, a smaller 0.20 eV gap is identified 1.05 eV below the Fermi level located only in the bottom graphene layer. In contrast, the top graphene layer is gapless, and nearly indistinguishable from the pristine monolayer graphene. The latter structure is in good agreement with the experimental data shown in Figure 2, particularly in the region where the top- and bottom-layer derived bands cross at finite momentum (red arrows in Figures 2D, F) and the Dirac point of the top graphene layer (blue arrows in Figures 2D, F), in agreement with our experimental ARPES results which show Ca-QFSBLG as AA-stacked.

The interaction distance between intercalated calcium atoms and graphene plays a crucial role in driving the electronic structure differences between AA-stacked and AB-stacked systems. In the AA-stacked system with calcium intercalation, we observed a larger separation between the graphene layers and calcium atoms for AA-stacked configuration (2.45 Å) in comparison to the AB-stacked configuration (2.33 Å, Supplementary Figure S3). This observation may provide a partial explanation for the diminished impact on the top layer during the doping process.

4 Conclusion

Calcium intercalation was successfully achieved in quasi-freestanding bilayer graphene on hydrogenated SiC, resulting in significant changes to the system. Upon calcium intercalation, calcium replaced hydrogen at the SiC interface, leading to a switch from p-type doping to n-type doping. This transition was accompanied with almost two orders of magnitude change in the carrier concentration, going from $n_h^{total} = 5.17 \times 10^{12}$ cm^{-2} to $n_e^{total} = 1.37 \times 10^{14}$ cm^{-2}, while retaining the quasi-freestanding nature, and exhibiting minimal change of the Fermi velocity. Structurally, the intercalation process resulted in a transformation from AB-stacked to AA-stacked bilayer graphene, a shift facilitated by a small difference in the formation energy between the two stacking types. As a result, the electronic band structure is significantly altered. The top layer of graphene is nearly indistinguishable from a pristine monolayer, retaining the ungapped Dirac point. While previous reports show indirect evidence of inhomogeneous AA- and AB-stacked regions in epitaxial graphene following lithium intercalation and de-intercalation, to our knowledge, this is the first report of the preparation of large-area, uniform quasi-freestanding AA-stacked graphene following calcium intercalation. This opens the door to further study of the properties of this distinct new graphene system with its unique band structure.

Data availability statement

The datasets presented in this study can be found in online repositories. The names of the repository/repositories and accession number(s) can be found below: Zenodo: https://doi.org/10.5281/zenodo.10071225.

Author contributions

AG-C: Formal Analysis, Investigation, Visualization, Writing–original draft, Writing–review and editing, Conceptualization. JK: Conceptualization, Investigation, Writing–review and editing. YY: Formal Analysis, Writing–review and editing. AT: Data curation, Formal Analysis, Investigation, Resources, Software, Writing–review and editing. MH: Investigation, Writing–review and editing. SS: Investigation, Writing–review and editing. JR: Data curation, Resources, Writing–review and editing. EH: Resources, Writing–review and editing. KD: Resources, Writing–review and editing. RM-W: Resources, Writing–review and editing. ME: Investigation, Supervision, Writing–review and editing. NM: Formal Analysis, Supervision, Writing–review and editing. DG: Resources, Supervision, Writing–review and editing. MF: Conceptualization, Funding acquisition, Supervision, Writing–original draft, Writing–review and editing, Project administration.

Funding

The author(s) declare financial support was received for the research, authorship, and/or publication of this article. This work was supported by the Australian Research Council under awards DP150103837, DP200101345 and FL120100038. JK was supported by the Australian Government Research Training Program, and the Monash Centre for Atomically Thin Materials. YY and NM were supported by the Australian Research Council (CE17010039). DG, RM-W, and KD were supported by core programs at the U.S. Naval Research Laboratory funded by the Office of Naval Research.

Acknowledgments

This research was undertaken on the Soft X-ray spectroscopy beamline at the Australian Synchrotron, part of ANSTO. YY and NM gratefully acknowledge the computational support from the National Computing Infrastructure and Pawsey Supercomputing Facilities. Preprint version of this article was published on arXiv repository as Grubišić-Čabo et al. (2023).

Conflict of interest

The authors declare that the research was conducted in the absence of any commercial or financial relationships that could be construed as a potential conflict of interest.

Publisher's note

All claims expressed in this article are solely those of the authors and do not necessarily represent those of their affiliated organizations, or those of the publisher, the editors and the reviewers. Any product that may be evaluated in this article, or claim that may be made by its manufacturer, is not guaranteed or endorsed by the publisher.

Supplementary material

The Supplementary Material for this article can be found online at: https://www.frontiersin.org/articles/10.3389/fnano.2023.1333127/full#supplementary-material

References

Bao, W., Wan, J., Han, X., Cai, X., Zhu, H., Kim, D., et al. (2014). Approaching the limits of transparency and conductivity in graphitic materials through lithium intercalation. *Nat. Commun.* 5, 4224. doi:10.1038/ncomms5224

Briggs, N., Gebeyehu, Z. M., Vera, A., Zhao, T., Wang, K., De La Fuente Duran, A., et al. (2019). Epitaxial graphene/silicon carbide intercalation: a minireview on graphene modulation and unique 2D materials. *Nanoscale* 11, 15440–15447. doi:10.1039/C9NR03721G

Broekman, L., Tadich, A., Huwald, E., Riley, J., Leckey, R., Seyller, T., et al. (2005). First results from a second generation toroidal electron spectrometer. *J. Electron Spectrosc. Relat. Phenom.* 144-147, 1001–1004. doi:10.1016/j.elspec.2005.01.022

Caffrey, N. M., Johansson, L. I., Xia, C., Armiento, R., Abrikosov, I. A., and Jacobi, C. (2016). Structural and electronic properties of Li-intercalated graphene on SiC(0001). *Phys. Rev. B* 93, 195421. doi:10.1103/PhysRevB.93.195421

Chen, M., and Weinert, M. (2018). Layer *k*-projection and unfolding electronic bands at interfaces. *Phys. Rev. B* 98, 245421. doi:10.1103/PhysRevB.98.245421

Chen, M. X., Chen, W., Zhang, Z., and Weinert, M. (2017). Effects of magnetic dopants in $Li_{0.8}M_{0.2}OH$ FeSe (M=Fe, Mn, Co): density functional theory study using a band unfolding technique. *Phys. Rev. B* 96, 245111. doi:10.1103/PhysRevB.96.245111

Damascelli, A. (2004). Probing the electronic structure of complex systems by ARPES. *Phys. Scr.* T109, 61. doi:10.1238/Physica.Topical.109a00061

Daniels, K. M., Jadidi, M. M., Sushkov, A. B., Nath, A., Boyd, A. K., Sridhara, K., et al. (2017). Narrow plasmon resonances enabled by quasi-freestanding bilayer epitaxial graphene. *2D Mat.* 4, 025034. doi:10.1088/2053-1583/aa5c75

de Jong, T. A., Krasovskii, E. E., Ott, C., Tromp, R. M., van der Molen, S. J., and Jobst, J. (2018). Intrinsic stacking domains in graphene on silicon carbide: a pathway for intercalation. *Phys. Rev. Mat.* 2, 104005. doi:10.1103/PhysRevMaterials.2.104005

de Jong, T. A., Visser, L., Jobst, J., Tromp, R. M., and van der Molen, S. J. (2023). Stacking domain morphology in epitaxial graphene on silicon carbide. *Phys. Rev. Mat.* 7, 034001. doi:10.1103/PhysRevMaterials.7.034001

Elias, D. C., Gorbachev, R. V., Mayorov, A. S., Morozov, S. V., Zhukov, A. A., Blake, P., et al. (2011). Dirac cones reshaped by interaction effects in suspended graphene. *Nat. Phys.* 7, 701–704. doi:10.1038/nphys2049

Emery, N., Hérold, C., d'Astuto, M., Garcia, V., Bellin, C., Marêché, J. F., et al. (2005). Superconductivity of bulk CaC_6. *Phys. Rev. Lett.* 95, 087003. doi:10.1103/PhysRevLett.95.087003

Emtsev, K. V., Bostwick, A., Horn, K., Jobst, J., Kellogg, G. L., Ley, L., et al. (2009). Towards wafer-size graphene layers by atmospheric pressure graphitization of silicon carbide. *Nat. Mat.* 8, 203–207. doi:10.1038/nmat2382

Emtsev, K. V., Speck, F., Seyller, T., Ley, L., and Riley, J. D. (2008). Interaction, growth, and ordering of epitaxial graphene on SiC{0001} surfaces: a comparative photoelectron spectroscopy study. *Phys. Rev. B* 77, 155303. doi:10.1103/PhysRevB.77.155303

Endo, Y., Fukaya, Y., Mochizuki, I., Takayama, A., Hyodo, T., and Hasegawa, S. (2020). Structure of superconducting Ca-intercalated bilayer graphene/SiC studied using total-reflection high-energy positron diffraction. *Carbon* 157, 857–862. doi:10.1016/j.carbon.2019.10.070

Endo, Y., Ichinokura, S., Akiyama, R., Takayama, A., Sugawara, K., Nomura, K., et al. (2018). Weak localization in bilayer graphene with Li-intercalation/desorption. *J. Phys. Condens. Matter.* 30, 305701. doi:10.1088/1361-648x/aaccc4

Grimme, S., Ehrlich, S., and Goerigk, L. (2011). Effect of the damping function in dispersion corrected density functional theory. *J. Comput. Chem.* 32, 1456–1465. doi:10.1002/jcc.21759

Grubišić-Čabo, A., Kotsakidis, J. C., Yin, Y., Tadich, A., Haldon, M., Solari, S., et al. (2021). Magnesium-intercalated graphene on SiC: highly n-doped air-stable bilayer graphene at extreme displacement fields. *Appl. Surf. Sci.* 541, 148612. doi:10.1016/j.apsusc.2020.148612

Grubišić-Čabo, A., Kotsakidis, J. C., Yin, Y., Tadich, A., Haldon, M., Solari, S., et al. (2023). Quasi-free-standing AA-stacked bilayer graphene induced by calcium intercalation of the graphene-silicon carbide interface. *arXiv.* 2311.02528.

Hwang, C., Park, C.-H., Siegel, D. A., Fedorov, A. V., Louie, S. G., and Lanzara, A. (2011). Direct measurement of quantum phases in graphene via photoemission spectroscopy. *Phys. Rev. B* 84, 125422. doi:10.1103/PhysRevB.84.125422

Hwang, C., Siegel, D. A., Mo, S.-K., Regan, W., Ismach, A., Zhang, Y., et al. (2012). Fermi velocity engineering in graphene by substrate modification. *Sci. Rep.* 2, 590. doi:10.1038/srep00590

Ichinokura, S., Sugawara, K., Takayama, A., Takahashi, T., and Hasegawa, S. (2016). Superconducting calcium-intercalated bilayer graphene. *ACS Nano* 10, 2761–2765. doi:10.1021/acsnano.5b07848

Kanetani, K., Sugawara, K., Sato, T., Shimizu, R., Iwaya, K., Hitosugi, T., et al. (2012). Ca intercalated bilayer graphene as a thinnest limit of superconducting C_6Ca. *PNAS* 109, 19610–19613. doi:10.1073/pnas.1208889109

Katsnelson, M. I., Novoselov, K. S., and Geim, A. K. (2006). Chiral tunnelling and the Klein paradox in graphene. *Nat. Phys.* 2, 620–625. doi:10.1038/nphys384

Kim, H., Dugerjav, O., Lkhagvasuren, A., and Seo, J. M. (2019). Doping modulation of quasi-free-standing monolayer graphene formed on SiC(0001) through $Sn_{1-x}Ge_x$ intercalation. *Carbon* 144, 549–556. doi:10.1016/j.carbon.2018.12.084

Kim, K. S., Warlter, A. L., Moreschini, L., Seyller, T., Horn, K., Rotenberg, E., et al. (2013). Coexisting massive and massless Dirac fermions in symmetry-broken bilayer graphene. *Nat. Mat.* 12, 887–892. doi:10.1038/nmat3717

Kotsakidis, J. C., Currie, M., Grubišić-Čabo, A., Tadich, A., Myers-Ward, R. L., DeJarld, M., et al. (2021). Increasing the rate of magnesium intercalation underneath epitaxial graphene on 6H-SiC(0001). *Adv. Mat. Interfaces* 8, 2101598. doi:10.1002/admi.202101598

Kotsakidis, J. C., Grubišić-Čabo, A., Yin, Y., Tadich, A., Myers-Ward, R. L., DeJarld, M., et al. (2020). Freestanding n-doped graphene via intercalation of calcium and magnesium into the buffer layer–SiC(0001) interface. *Chem. Mat.* 32, 6464–6482. doi:10.1021/acs.chemmater.0c01729

Kresse, G., and Furthmüller, J. (1996). Efficiency of ab-initio total energy calculations for metals and semiconductors using a plane-wave basis set. *Comput. Mat. Sci.* 6, 15–50. doi:10.1016/0927-0256(96)00008-0

Kruskopf, M., Pakdehi, D. M., Pierz, K., Wundrack, S., Stosch, R., Dziomba, T., et al. (2016). Comeback of epitaxial graphene for electronics: large-area growth of bilayer-free graphene on SiC. *2D Mat.* 3, 041002. doi:10.1088/2053-1583/3/4/041002

Li, G., Luican, A., Lopes dos Santos, J. M. B., Castro Neto, A. H., Reina, A., Kong, J., et al. (2010). Observation of van Hove singularities in twisted graphene layers. *Nat. Phys.* 6, 109–113. doi:10.1038/nphys1463

Liu, Y., Bian, G., Miller, T., and Chiang, T.-C. (2011). Visualizing electronic chirality and Berry phases in graphene systems using photoemission with circularly polarized light. *Phys. Rev. Lett.* 107, 166803. doi:10.1103/PhysRevLett.107.166803

Liu, Z., Suenaga, K., Harris, P. J. F., and Iijima, S. (2009). Open and closed edges of graphene layers. *Phys. Rev. Lett.* 102, 015501. doi:10.1103/PhysRevLett.102.015501

Marchenko, D., Varykhalov, A., Sánchez-Barriga, J., Seyller, T., and Rader, O. (2016). Rashba splitting of 100 meV in Au-intercalated graphene on SiC. *Appl. Phys. Lett.* 108, 172405. doi:10.1063/1.4947286

Mazin, I., and Balatsky, A. (2010). Superconductivity in Ca-intercalated bilayer graphene. *Philos. Mag. Lett.* 90, 731–738. doi:10.1080/09500839.2010.487473

McCann, E., and Koshino, M. (2013). The electronic properties of bilayer graphene. *Rep. Prog. Phys.* 76, 056503. doi:10.1088/0034-4885/76/5/056503

McChesney, J. L., Bostwick, A., Ohta, T., Seyller, T., Horn, K., González, J., et al. (2010). Extended van Hove singularity and superconducting instability in doped graphene. *Phys. Rev. Lett.* 104, 136803. doi:10.1103/PhysRevLett.104.136803

Novoselov, K., Geim, A., Morozov, S., Jiang, D., Zhang, Y., Dubonos, S., et al. (2004). Electric field effect in atomically thin carbon films. *Science* 80, 306666–306669. doi:10.1126/science.1102896

Novoselov, K. S., Geim, A. K., Morozov, S. V., Jiang, D., Katsnelson, M. I., Grigorieva, I. V., et al. (2005). Two-dimensional gas of massless Dirac fermions in graphene. *Nature* 438, 197–200. doi:10.1038/nature04233

Novoselov, K. S., McCann, E., Morozov, S. V., Fal'ko, V. I., Katsnelson, M. I., Zeitler, U., et al. (2006). Unconventional quantum Hall effect and Berry's phase of 2π in bilayer graphene. *Nat. Phys.* 2, 177–180. doi:10.1038/nphys245

Nyakiti, L., Wheeler, V., Garces, N., Myers-Ward, R., Eddy, C., and Gaskill, D. (2012). Enabling graphene-based technologies: toward wafer-scale production of epitaxial graphene. *MRS Bull.* 37, 1149–1157. doi:10.1557/mrs.2012.180

Ohta, T., Bostwick, A., Seyller, T., Horn, K., and Rotenberg, E. (2006). Controlling the electronic structure of bilayer graphene. *Science* 313, 951–954. doi:10.1126/science.1130681

Oliveira, M. H., Schumann, T., Fromm, F., Koch, R., Ostler, M., Ramsteiner, M., et al. (2013). Formation of high-quality quasi-free-standing bilayer graphene on SiC(0001) by oxygen intercalation upon annealing in air. *Carbon* 52, 83–89. doi:10.1016/j.carbon.2012.09.008

Partoens, B., and Peeters, F. M. (2006). From graphene to graphite: electronic structure around the *K* point. *Phys. Rev. B* 74, 075404. doi:10.1103/PhysRevB.74.075404

Perdew, J. P., Burke, K., and Ernzerhof, M. (1996). Generalized gradient approximation made simple. *Phys. Rev. Lett.* 77, 3865–3868. doi:10.1103/PhysRevLett.77.3865

Riedl, C., Coletti, C., Iwasaki, T., Zakharov, A. A., and Starke, U. (2009). Quasi-free-standing epitaxial graphene on SiC obtained by hydrogen intercalation. *Phys. Rev. Lett.* 103, 246804. doi:10.1103/PhysRevLett.103.246804

Rozhkov, A., Sboychakov, A., Rakhmanov, A., and Nori, F. (2016). Electronic properties of graphene-based bilayer systems. *Phys. Rep.* 648, 1–104. doi:10.1016/j.physrep.2016.07.003

Sboychakov, A. O., Rakhmanov, A. L., Rozhkov, A. V., and Nori, F. (2021). Bilayer graphene can become a fractional metal. *Phys. Rev. B* 103, L081106. doi:10.1103/PhysRevB.103.L081106

Sforzini, J., Nemec, L., Denig, T., Stadtmüller, B., Lee, T.-L., Kumpf, C., et al. (2015). Approaching truly freestanding graphene: the structure of hydrogen-intercalated graphene on 6H-SiC(0001). *Phys. Rev. Lett.* 114, 106804. doi:10.1103/PhysRevLett.114.106804

Shen, K., Sun, H., Hu, J., Hu, J., Liang, Z., Li, H., et al. (2018). Fabricating quasi-free-standing graphene on a SiC(0001) surface by steerable intercalation of iron. *J. Phys. Chem. C* 122, 21484–21492. doi:10.1021/acs.jpcc.8b06789

Sohn, Y., Shin, W. J., Ryu, S. H., Huh, M., Cha, S., and Kim, K. S. (2021). Graphene p-n junction formed on SiC(0001) by Au intercalation. *J. Korean Phys. Soc.* 78, 40–44. doi:10.1007/s40042-020-00010-0

Starke, U., and Riedl, C. (2009). Epitaxial graphene on SiC(0001) and SiC(000$\bar{1}$): from surface reconstructions to carbon electronics. *J. Condens. Matter Phys.* 21, 134016. doi:10.1088/0953-8984/21/13/134016

Sugawara, K., Sato, T., and Takahashi, T. (2009). Fermi-surface-dependent superconducting gap in C_6Ca. *Nat. Phys.* 5, 40–43. doi:10.1038/nphys1128

Sung, S. J., Yang, J. W., Lee, P. R., Kim, J. G., Ryu, M. T., Park, H. M., et al. (2014). Spin-induced band modifications of graphene through intercalation of magnetic iron atoms. *Nanoscale* 6, 3824–3829. doi:10.1039/C3NR04178F

Toyama, H., Akiyama, R., Ichinokura, S., Hashizume, M., Iimori, T., Endo, Y., et al. (2022). Two-dimensional superconductivity of Ca-intercalated graphene on SiC: vital role of the interface between monolayer graphene and the substrate. *ACS Nano* 16, 3582–3592. doi:10.1021/acsnano.1c11161

Valla, T., Camacho, J., Pan, Z.-H., Fedorov, A. V., Walters, A. C., Howard, C. A., et al. (2009). Anisotropic electron-phonon coupling and dynamical nesting on the graphene sheets in superconducting CaC_6 using angle-resolved photoemission spectroscopy. *Phys. Rev. Lett.* 102, 107007. doi:10.1103/PhysRevLett.102.107007

Virojanadara, C., Watcharinyanon, S., Zakharov, A. A., and Johansson, L. I. (2010). Epitaxial graphene on 6*H*-SiC and Li intercalation. *Phys. Rev. B* 82, 205402. doi:10.1103/PhysRevB.82.205402

Watcharinyanon, S., Johansson, L., Zakharov, A. A., and Virojanadara, C. (2012). Studies of Li intercalation of hydrogenated graphene on SiC(0001). *Surf. Sci.* 606, 401–406. doi:10.1016/j.susc.2011.10.023

Watcharinyanon, S., Johansson, L. I., Xia, C., and Virojanadara, C. (2013). Ytterbium oxide formation at the graphene–SiC interface studied by photoemission. *J. Vac. Sci. Technol. A* 31, 020606. doi:10.1116/1.4792040

Weller, T. E., Ellerby, M., Saxena, S. S., Smith, R. P., and Skipper, N. T. (2005). Superconductivity in the intercalated graphite compounds C_6Yb and C_6Ca. *Nat. Phys.* 1, 39–41. doi:10.1038/nphys0010

Wolff, S., Roscher, S., Timmermann, F., Daniel, M. V., Speck, F., Wanke, M., et al. (2019). Quasi-freestanding graphene on SiC(0001) by Ar-mediated intercalation of antimony: a route toward intercalation of high-vapor-pressure elements. *Ann. Phys.* 531, 1900199. doi:10.1002/andp.201900199

Yang, S.-L., Sobota, J. A., Howard, C. A., Pickard, C. J., Hashimoto, M., Lu, D. H., et al. (2014). Superconducting graphene sheets in CaC_6 enabled by phonon-mediated interband interactions. *Nat. Commun.* 5, 3493. doi:10.1038/ncomms4493

Zhang, P., Richard, P., Qian, T., Xu, Y.-M., Dai, X., and Ding, H. (2011). A precise method for visualizing dispersive features in image plots. *Rev. Sci. Instrum.* 82, 043712. doi:10.1063/1.3585113

Zhang, Y., Tan, Y.-W., Stormer, H. L., and Kim, P. (2005). Experimental observation of the quantum Hall effect and Berry's phase in graphene. *Nature* 438, 201–204. doi:10.1038/nature04235